

Extending “color constancy” outside the visible region

Sivalogeswaran Ratnasingam,^{1,*} Steve Collins,¹ and Javier Hernández-Andrés²

¹*Department of Engineering Science, University of Oxford, OX1 3PJ, Oxford, UK*

²*Department of Optics, Sciences Faculty, University of Granada, Granada, 18071, Spain*

*Corresponding author: siva@robots.ox.ac.uk

Received January 4, 2011; accepted January 26, 2011;
posted January 31, 2011 (Doc. ID 140547); published March 10, 2011

In this paper, the results of an investigation of the possibility of extending “color constancy” to obtain illuminant-invariant reflectance features from data in the near-ultraviolet (UV) and near-infrared (IR) wavelength regions are reported. These features are obtained by extending a blackbody-model-based color constancy algorithm proposed by Ratnasingam and Collins [J. Opt. Soc. Am. A **27**, 286 (2010)] to these additional wavelengths. Ratnasingam and Collins applied the model-based algorithm in the visible region to extract two illuminant-invariant features related to the wavelength-dependent reflectance of a surface from the responses of four sensors. In this paper, this model-based algorithm is extended to extract two illuminant-invariant reflectance features from the responses of sensors that cover the visible and either the near-UV or near-IR wavelength. In this investigation, test reflectance data sets are generated using the goodness–fitness coefficient (GFC). The appropriateness of the GFC for generating the test data sets is demonstrated by comparing the results obtained with these data with those obtained from data sets generated using the CIE Lab distance. Results based upon the GFC are then presented that suggest that the model-based algorithm can extract useful features from data from the visible and near-IR wavelengths. Finally, results are presented that show that, although the spectrum of daylight in the near UV is very different from a blackbody spectrum, the algorithm can be modified to extract useful features from visible and near-UV wavelengths.

© 2011 Optical Society of America

OCIS codes: 330.0330, 330.1690, 330.1720, 330.1730.

1. INTRODUCTION

The wavelength-dependent reflectance of an object is an important property that is used by the human visual system to recognize objects independent of the viewing environment, including variation in illuminating light. This is possible for the human visual system because of its ability to perceive color largely independent of the illuminant. In the past, researchers have modeled the human visual system and proposed several different approaches to obtain illuminant-invariant features from a scene. Most of these approaches make assumptions either about the scene or the illuminant or the image sensor or a combination of all the factors. For example, von Kries first proposed an adaptation model for the human visual system known as the coefficient rule, which is widely applied for solving color constancy [1,2]. However, this model assumes that the image sensors have nonoverlapping narrowband sensitivity functions [1]. A computational model has been proposed by Land and McCann [3]. This model uses the logarithm of sensor responses in processing for color constancy. A blackbody model of illuminant assumption has been made by Marchant and Onyango [4], and they proposed an approach for obtaining illuminant-invariant features from a scene. Finlayson and co-workers [5,6] proposed color constancy algorithms based on the assumptions that the image sensors sample the scene at a single wavelength, and the illuminant power spectrum can be modeled by a blackbody spectrum. Recently, Ratnasingam and Collins [7] proposed a relatively simple blackbody-model-based algorithm for obtaining two illuminant-invariant features in the visible spectrum using four sensor responses. This algorithm is also based on the assumptions that the image sensors are infinitely narrow, and the

power spectrum of an illuminant can be approximated using a blackbody spectrum.

All of this previous work has focussed on the visible wavelengths. However, there are other applications, including remote sensing of the soil types, minerals, terrestrial vegetation, man-made materials, snow cover fraction, and melting of snow, for which the reflectance properties of surfaces outside the visible region can be very useful. In these remote sensing applications, the tone (the relative brightness of an area at different wavelengths) is used as the fundamental feature for distinguishing different targets [8]. Generally, in remote sensing applications, the interpretation and identification of different regions are performed manually [8]. An important capability that is required before this process can be automated is to be able to analyze multiple images of the same region taken at different times. This can only be achieved if the impact of the changes in the power spectral density of the daylight illuminant at different times can be minimized. These variations could be removed by extracting illuminant-invariant reflectance dependent features using the method proposed by Ratnasingam and Collins [7]. This proposed algorithm has been used to extract illuminant-invariant chromaticity features using data from the visible region. In the current paper, the possibility of extending this algorithm to extract illuminant-invariant reflectance features from a wider wavelength range is investigated.

Section 2 briefly describes the blackbody-model-based algorithm and the assessment method adapted from Ratnasingam and Collins [7]. The spectral variation of the measured daylight in Granada, Spain, is illustrated in Section 3. Generation of a test data set in different wavelength ranges and the metric used to generate the data set are discussed in Section 4.

Section 5 illustrates the results and discussion on the results. Finally, conclusions are made in Section 6.

2. EXTRACTION OF ILLUMINANT-INVARIANT REFLECTANCE FEATURES

The blackbody-model-based algorithm proposed by Ratnasingam and Collins [7] can be used to extract two illuminant-invariant reflectance-dependent features from four sensor responses. Similar to other researchers [4,5], for mathematical simplicity, Ratnasingam and Collins [7] assumed that the power spectral density of an illuminant can be modeled by a blackbody spectrum and that the imaging sensors each sample the scene at a different single wavelength. Based on these two assumptions, Ratnasingam and Collins [7] derived two illuminant-invariant features (F_1 and F_2),

$$F_1 = \log(R_2) - \{\alpha \log(R_1) + (1 - \alpha) \log(R_3)\}, \quad (1)$$

$$F_2 = \log(R_3) - \{\gamma \log(R_2) + (1 - \gamma) \log(R_4)\}, \quad (2)$$

from four image sensor responses (R_1, R_2, R_3 , and R_4), where α and γ are the channel coefficients. Variations in the image sensor responses caused by the illuminant intensity and illuminant spectral power distribution can be removed if the two channel coefficients (α and γ) satisfy the following equations [7]:

$$\frac{1}{\lambda_2} = \frac{\alpha}{\lambda_1} + \frac{1 - \alpha}{\lambda_3}, \quad (3)$$

$$\frac{1}{\lambda_3} = \frac{\gamma}{\lambda_2} + \frac{1 - \gamma}{\lambda_4}, \quad (4)$$

where $\lambda_1, \lambda_2, \lambda_3$, and λ_4 are the wavelengths at which the sensor's response is maximal.

The assumption that the sensors respond at a single wavelength is technologically difficult to achieve with real sensors. In addition, sensors with a very narrow spectral sensitivity will be starved of photons, and this will result in low sensitivity and require a long integration time. These problems mean that it is important to investigate the performance of the model-based algorithm [7] with data from sensors that respond to significant wavelength ranges. To investigate this effect, Ratnasingam and Collins [7] modeled the sensors' spectral sensitivity functions using Gaussian functions of different full-widths at half-maximum (FWHMs) and concluded that the algorithm can be used to extract useful illuminant-invariant features with image sensors of 80 nm FWHM or less. Because cameras such as the Sony DXC930 exist with three sensors that are sensitive to wavelengths in a range of ~ 80 nm spectral width, we are particularly interested in investigating the performance of the algorithm with sensors that respond to wavelength ranges of around 80 nm in width. Ratnasingam and co-workers [7,9] later concluded that the algorithm can be used to extract illuminant-invariant features from scenes illuminated by daylight.

Similar to Ratnasingam and Collins [7], to obtain realistic results, sensor noise and quantization noise have been included in this study. Winkler and Susstrunk's [10] empirical results show that imagers are available with a signal-to-noise ratio (SNR) larger than 40 dB. Based on this evidence, the

model-based algorithm was investigated with simulated sensor responses that have an SNR of 40 dB. In the simulations, this SNR was achieved by multiplying each ideal sensor response by 100 random numbers sampled from a Gaussian distribution that has a mean value of 1 and a standard deviation of 1%. Each of the 100 noisy responses was then quantized to 10 bits [7].

Ratnasingam and Collins [7] have shown that the two-dimensional feature space formed from the two extracted features shows a smooth variation of "color" across the feature space. However, due to noise and imperfect cancellation of the changes in the illuminant spectrum, each surface creates a small cluster of points in this space. To investigate the effect of these clusters, Ratnasingam and Collins [7] proposed an assessment method based upon the Mahalanobis distance measure. This method is based upon pairs of clusters formed by two reflectances when illuminated by a training illuminant set. The first step in this assessment method is to calculate the Mahalanobis distances between the centers of each cluster (C_1 and C_2) and the midpoint (P) of the line connecting these two points. If D_{m1} is the Mahalanobis distance of P from C_1 and D_{m2} is the Mahalanobis distance between P and C_2 , then

$$D_{m1}^2 = (P - C_1)' \Sigma_1^{-1} (P - C_1), \quad (5)$$

$$D_{m2}^2 = (P - C_2)' \Sigma_2^{-1} (P - C_2), \quad (6)$$

where Σ_1^{-1} and Σ_2^{-1} are the inverse covariance matrices of clusters 1 and 2, respectively.

These distances are then used to determine boundaries around the two clusters that can be used to determine cluster membership. If these boundaries are drawn using D_{m1} and D_{m2} , then, as shown in Fig. 1(a), there can be overlap between the clusters. To avoid any overlap between Mahalanobis distance boundaries formed by a pair of reflectances and to reduce the complexity of finding the correct boundary for this study, the Mahalanobis distance boundary has been obtained using 90% of D_{m1} and D_{m2} . Inspection of each of the resulting cluster boundaries showed that the boundaries drawn with 90% of D_{m1} and D_{m2} , see a typical boundary in Fig. 1(b), are nonoverlapping and will slightly underestimate the ability to correctly assign a point to the correct cluster. Once the boundaries are determined, a second set of illuminants (the test set) was used to illuminate the same reflectance pair and project the extracted noisy features onto the 2D space. The separability of this pair is then determined by counting the number of points that fall inside the correct boundary. This procedure was repeated for all the pairs in the reflectance set, and the percentage of separability was calculated.

In assessing the performance of the algorithm, Munsell [11], floral [12], and measured daylight [13] have been used. The measured daylight spectra are available for wavelengths between 300 and 1100 nm [13]. As described by Ratnasingam and Collins [7], two sets of 146 spectra have been chosen from these measured daylight spectra. The first set of spectra were obtained by taking the spectra measured during the first day of each month of 1996, and the second set was generated by taking the daylight measured in the first day of each month of 1997. The sensor sensitivity functions of the image sensors were modeled by Gaussian functions. To ensure that data from all wavelengths are used in calculating the

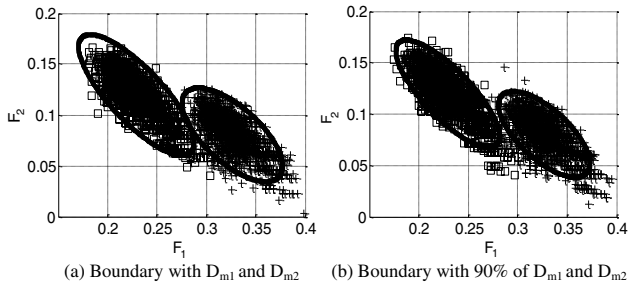


Fig. 1. Typical boundary of a reflectance pair from Munsell reflectance test set: (a) boundaries go through the midpoint of the two clusters' mean points and (b) boundaries drawn with 90% of the Mahalanobis distance (D_{m1} and D_{m2}). The Gaussian sensor responses were multiplied by 100 samples of 40 dB noise. In the figures, a square represents the points generated by one member of the reflectance pair, and a cross represents the points generated by the other member of the reflectance pair.

illuminant-invariant features, the wavelengths at which the four Gaussian functions peak were spread evenly over the wavelength range of interest. The separability results were then obtained with the FWHM of the Gaussian sensitivity functions varying from 20 to 200 nm.

3. CORRELATED COLOR TEMPERATURE VARIATION OF DAYLIGHT AND APPROXIMATION OF THE BLACKBODY MODEL BEYOND THE VISIBLE REGION

Outdoor scenes are illuminated by daylight, and a variety of effects means that the power spectral density of daylight changes. These changes in the power spectral density of daylight have been studied by measuring 2600 spectra over a period of two years under different weather conditions [13]. The possible effect of these changes in power spectral density on the apparent color of a surface can be appreciated by inspecting a few of these spectra in Fig. 2. The large shift in power to shorter wavelengths, shown in this figure as the correlated color temperature (CCT) of the daylight increases, can cause large changes in the apparent color of an object. These changes make it difficult to recognize objects based upon color information alone, and the aim of all color constancy algorithms is to minimize the effects of these changes.

The model-based algorithm relies on the assumption that the power spectrum of an illuminant can be modeled by a blackbody illuminant. Therefore, it is important to investigate whether the blackbody illuminant can be used to approximate the illuminant power spectrum when increasing the wavelength range of interest beyond the visible region. Figure 3 shows the power spectra of the blackbody illuminant and the measured daylight for the CCT value of 6557 K. From this typical figure, it can be seen that the blackbody illuminant approximates the power spectral density of daylight better in the near-infrared (IR) and visible regions of the spectrum than in the near-ultraviolet (UV) region. Therefore, the model-based algorithm is expected to give a better performance when applied to data from the visible and near-IR regions than when applied to data from the near-UV region.

4. GENERATION OF THE TEST DATA SET

From Fig. 3 it can be seen that daylight contains significant power at wavelengths longer than 300 nm. The performance

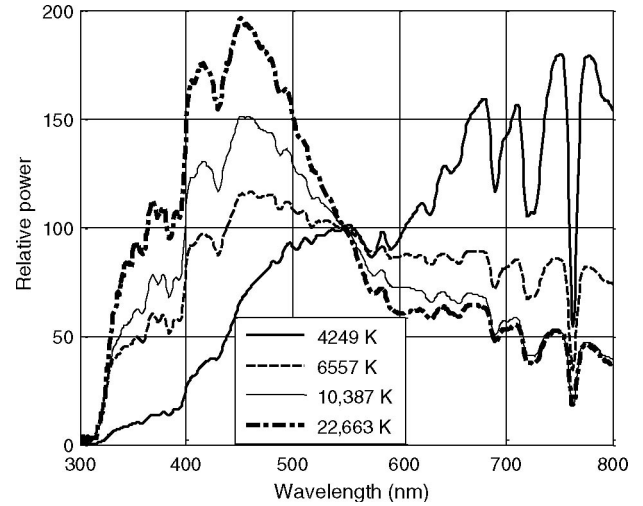


Fig. 2. Power spectra distribution of four of the measured daylight.

of the model-based algorithm was investigated by applying the sensor responses obtained from (i) the visible region alone (400 to 700 nm), (ii) visible and near-UV regions (300 to 700 nm), and (iii) visible and near-IR regions (400 to 800 nm). Munsell data are available in the wavelength range of 380 to 800 nm, and floral data are available in the wavelength range of 300 to 700 nm. Therefore, Munsell data were used to study the residual illuminant dependence of the features obtained from the model-based algorithm in the wavelength ranges of 400 to 700 and 400 to 800 nm. Floral reflectance data were used for the same study in the wavelength ranges of 300 to 700 and 400 to 700 nm.

A key part of the assessment method is to create data sets of pairs of reflectances with a known level of similarity. Previously, when assessing the features obtained in the visible region of the spectrum, CIE Lab coordinates have been used to characterize the level of similarity of the pairs of reflectances. To extend the assessment to the features obtained with data outside the visible region, another measure of similarity is required. Because the model-based algorithm extracts lightness normalized features that are dependent on the relative variation of the reflectance spectrum, an appropriate

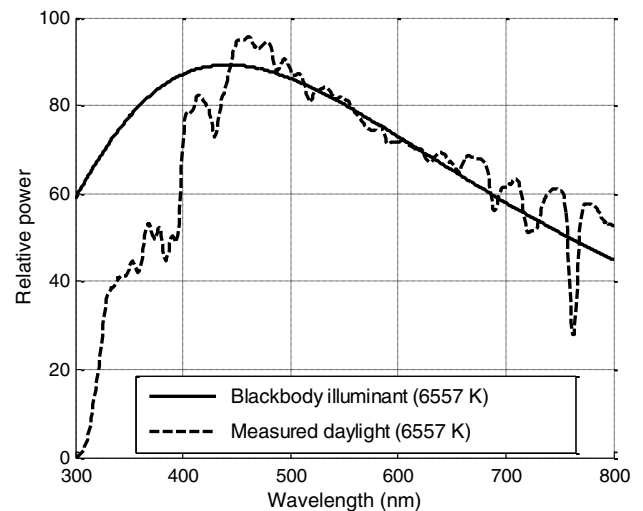


Fig. 3. Power spectra of blackbody illuminant (6557 K) and measured daylight (6557 K). Both spectra are normalized at 550 nm.

Table 1. Goodness-Fitness Coefficient Range of the Munsell and Floral Test Reflectance Data Sets for Different Wavelength Ranges

Wavelength Range	Nominal GFC Value of the Data Set	GFC Range of Munsell Test Set	GFC Range of Floral Test Set
400 to 700 nm	0.995	0.995 to 0.995013	0.995 to 0.995014
	0.999	0.999 to 0.999015	0.999 to 0.999019
400 to 800 nm	0.995	0.995 to 0.995009	—
	0.999	0.999 to 0.999015	—
300 to 700 nm	0.995	—	0.995 to 0.99498
	0.999	—	0.999 to 0.999134

measure of the similarity of two reflectances is the goodness-fitting coefficient (GFC) proposed by Romero *et al.* [14], which is widely used to measure the similarity between two spectra [14–17]. GFC is defined as follows:

$$\text{GFC} = \frac{\left| \sum_j E_E(\lambda_j) E_R(\lambda_j) \right|}{\left[\sum_j [E_E(\lambda_j)]^2 \right]^{1/2} \left[\sum_j [E_R(\lambda_j)]^2 \right]^{1/2}}, \quad (7)$$

where $E_E(\lambda)$ and $E_R(\lambda)$ are the reflectance spectra of two samples being compared. Previously, a pair of reflectances with a GFC > 0.995 has been defined as a colorimetrically good match, while a GFC > 0.999 is an excellent match [13]. Based on this criterion, two reflectance data sets were generated for each wavelength range. Each of these test data sets contains 100 pairs of reflectance spectra. In the first set, each pair of reflectances has a nominal GFC value of 0.995, while in the second data set, the nominal GFC value is 0.999. To obtain 100 pairs of reflectances for each data set, the range of GFC values used had to be changed slightly, and the particular ranges of GFC used in generating the test reflectance data sets from the Munsell and floral data sets are listed in Table 1.

To investigate the appropriateness of using the GFC to generate data sets for assessing the features obtained using the model-based algorithm, two sets of reflectance data sets were generated using the CIE Lab distance, according to the colorimetric interpretation in the wavelength range of 400 to 700 nm. As described by Ratnasingam and Collins [7], the

Munsell reflectance spectra were normalized in such a way that the L value is 50 units and two sets of 100 pairs of reflectances with member separation of 2.99 to 3.01 (three-unit data set) and 5.995 to 6.005 (six-unit data set). Similarly, two sets of 100 pairs of reflectances were chosen from the floral data set in such a way that the member separation between the pairs is 2.998 to 3.002 units and 5.998 to 6.001 units in the CIE Lab space. Results obtained using the reflectance data sets selected using either the GFC or the CIE Lab distance are shown in Fig. 4. These results show that there can be a significant difference between the results obtained with the data sets generated using GFC and the CIE Lab distance. However, in our investigation, we are interested in the overall trends in the results rather than the details of the results, which must depend upon the data set selected and the final application. For this study, the important conclusion from Fig. 4 is that the results obtained using data generated using the GFC show trends similar to the results obtained using data generated using the CIE Lab distance. Therefore, the GFC can be reliably used in assessing the usefulness of features obtained using the model-based algorithm when the sensors respond to wavelengths outside the visible region.

5. RESULTS AND DISCUSSION

To determine the usefulness of the features obtained from data in the visible and near IR, the model-based algorithm was tested for separability of reflectance samples that are similar in reflectance spectra by illuminating with 146 spectra of measured daylight in different wavelength ranges. For each of

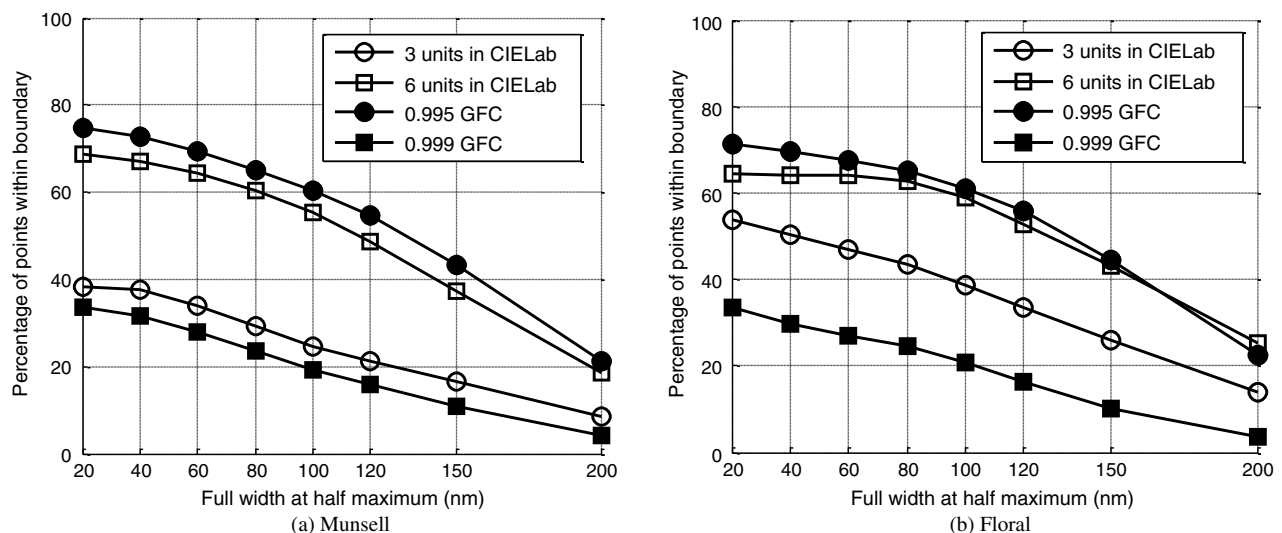


Fig. 4. Performance of the model-based algorithm when applying the reflectance data sets generated using GFC and CIE Lab distance: (a) Munsell and (b) floral. The algorithm was investigated by applying the data in the wavelength range of 400 to 700 nm.

Table 2. Channel Coefficients of the Model-Based Algorithm for Different Wavelength Ranges Calculated Using Eqs. (3) and (4)

Wavelength Range (nm)	Alpha	Gamma
400 to 700	0.427	0.436
300 to 700	0.389	0.409
400 to 800	0.409	0.423

these wavelength ranges, Gaussian sensitivity functions were placed in such a way that the sensitivity functions are evenly spread in the wavelength range of interest. The particular channel coefficients used in different wavelength ranges are listed in Table 2.

Figure 5 shows the performance of the model-based algorithm when tested with visible data alone and with visible and near-IR data together. Close investigation of the results obtained with both reflectance data sets shows a slight difference in performance improvement with both data sets. Particularly, a larger performance improvement was obtained when tested with a harder data set (GFC value of 0.999). Generally, when the performance of a system reaches above 75%, any further improvement requires a relatively larger effort. Therefore, the data set with a GFC of 0.995 shows a smaller improvement compared to the performance improvement obtained using a GFC of 0.999 reflectance data set. Noticeably, the reflectance data set with the GFC of 0.999 shows a significant performance improvement for the image sensor spectral width of 20 nm, while the reflectance data set with the GFC of 0.995 shows an insignificant improvement for a sensor width of 20 nm FWHM. This could be because when the sensors become narrow, the sensitivity functions do not cover the entire wavelength region with a significant sensitivity. Therefore, the sensor responses do not capture the entire differences between the reflectance pairs, and this leads to the difference in performance improvement between the two data sets with 20 nm FWHM sensors. The most important conclusion from the results in Fig. 6 is that the inclusion of data from the near IR has not degraded the results that have been obtained. This shows that, as expected, the model-based feature extraction method works well in the near IR, because the blackbody

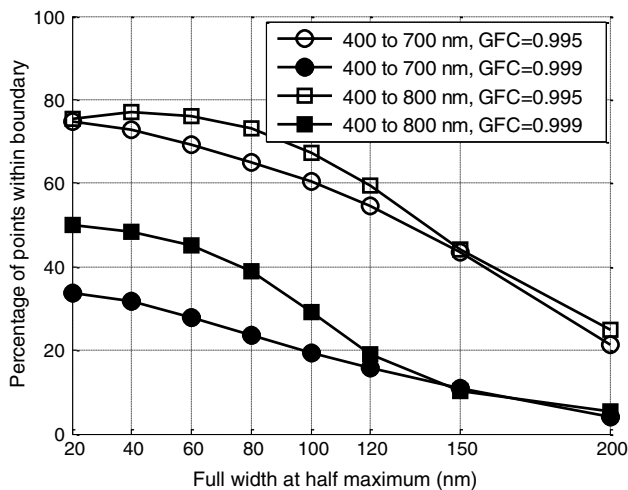


Fig. 5. Separability test results with Munsell and measured daylight. In this test, the model-based four-sensor algorithm was tested with visible data alone and visible and near-IR data together.

model approximates the daylight spectrum relatively well in the near-IR region. These results also suggest that including the near-IR data can make it easier to distinguish very similar reflectances. This is possibly because the wider wavelength range allows the sensor responses to be spread out so that overlap between the sensor responses is reduced. This will result in a lower correlation between the adjacent sensor responses, and this reduced correlation is known to improve the quality of the features that are obtained [7].

Figure 6 shows the results obtained using data from the visible region alone (400 to 700 nm) and visible and near-UV data together (300 to 700 nm). In this investigation, floral data sets were illuminated by 146 spectra of measured daylight. The results obtained, shown in Fig. 6, suggest that for narrowband sensors (FWHM < 75 nm), the separability of the data set with a GFC of 0.999 is improved when near-UV data are used. However, for wider sensors and these data set and the data set with a GFC of 0.995, the separability of pairs of reflectances has been reduced when data from the near UV are included.

The observed reduction in separability shown in Fig. 6 could occur because in the near UV, the power spectral distribution of daylight deviates significantly from the blackbody spectrum (see Fig. 3). Specifically, the measured daylight spectrum is significantly below the blackbody spectrum in the near-UV region. Therefore, assigning a larger value [larger than the value calculated using Eq. (3)] for the channel coefficient associated with the sensor that responds in the near-UV region might improve the features of 300 to 700 nm. To investigate this possibility, the channel coefficient alpha was varied in steps of 0.1 between 0 and 1 for each sensor width. The results obtained showed that the separability of the data was improved by increasing the value of alpha. For sensors with a FWHM larger than 120 nm, an alpha value of 0.7 gives the best results; however, the difference between the performance obtained for an alpha value of 0.7 and 0.8 is negligible. For sensors with a FWHM between 20 and 120 nm, peak performance was obtained for a channel coefficient of 0.8. This suggests that the optimum value of alpha is 0.8 rather than the calculated value of 0.389.

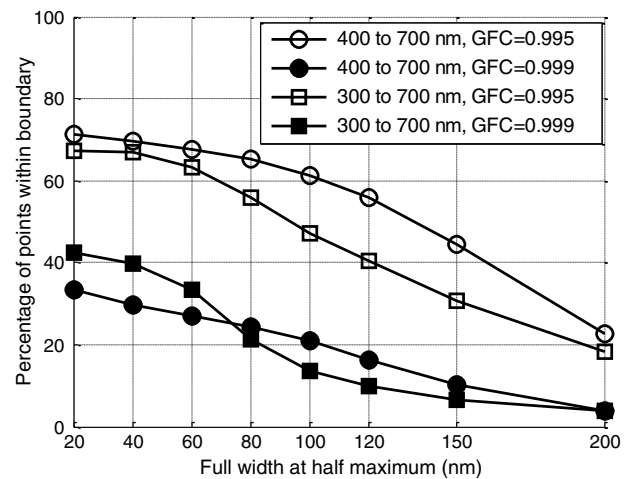


Fig. 6. Separability test results with floral and measured daylight. In this test, the model-based algorithm was tested with visible data alone and visible and UV data together.

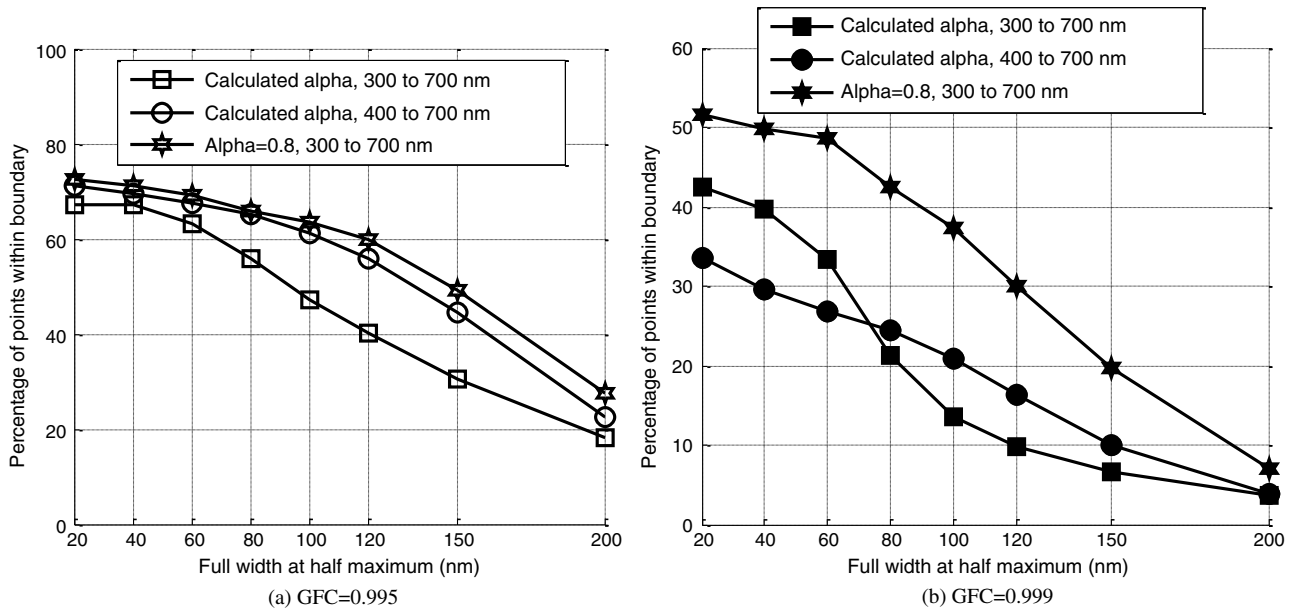


Fig. 7. Performance of the model-based algorithm with floral and measured daylight when tested with visible data alone and visible and UV data together with GFC values of (a) 0.995 and (b) 0.999. The performance of the algorithm with calculated coefficients (listed in Table 2) in the respective wavelength ranges and also the performance of the algorithm with an alpha value of 0.8 (optimum alpha). In all three cases, the channel coefficient gamma was kept the same as calculated (see Table 2).

Figure 7 shows a comparison between the results obtained using the calculated and the optimum value of alpha. This comparison shows that once the value of alpha is optimum, better results are obtained. Now the results are similar to the results in Fig. 5. Most importantly this shows that although the spectrum in the near UV is quite different from that expected from a blackbody, the feature extraction algorithm that was derived assuming a blackbody spectrum can be modified to obtain features including data from the near UV.

6. CONCLUSIONS

A color constancy algorithm has been applied to obtain illuminant-invariant reflectance features from different wavelength ranges. This algorithm extracts two illuminant-invariant features from four image sensor responses. The algorithm has been proposed assuming that the power spectral density of the illuminant is similar to that of a blackbody, and it has been tested using measured daylight spectra for visible wavelengths. The possibility of extending this algorithm to other wavelengths has been investigated by applying data from (i) the visible region alone, (ii) the visible and near-IR region, and (iii) the visible and near-UV regions, respectively. Results have been presented that show that stable illuminant-invariant features can be obtained using data from the visible and near-IR regions. Although the power spectral distribution of daylight in the near UV is quite different from the blackbody spectrum, only a slight modification to the algorithm can extract features from data in the near UV. In conclusion, the model-based algorithm can be used to obtain illuminant-invariant reflectance features in the near-IR, visible, and near-UV regions. As the human visual system does not have significant sensitivity to the near-UV and near-IR regions, these features cannot be used in applications in which the ultimate goal is visualizing the output. However, there are applications that use the data outside the

visible region and rely on tone/brightness to classify these data. For these kinds of applications, including remote sensing, this algorithm could be useful.

REFERENCES

1. J. A. Worthey and M. H. Brill, "Heuristic analysis of von Kries color constancy," *J. Opt. Soc. Am. A* **17**, 1708–1720 (1986).
2. M. Ebner, *Color Constancy*, Wiley-IS&T Series in Imaging Science and Technology (Wiley, 2007).
3. E. H. Land and J. J. McCann, "Lightness and retinex theory," *J. Opt. Soc. Am.* **61**, 1–11 (1971).
4. J. A. Marchant and C. M. Onyango, "Shadow-invariant classification for scenes illuminated by daylight," *J. Opt. Soc. Am. A* **17**, 1952–1961, 2000.
5. G. D. Finlayson and S. D. Hordley, "Color constancy at a pixel," *J. Opt. Soc. Am. A* **18**, 253–264, 2001.
6. G. D. Finlayson and M. S. Drew, "4-sensor camera calibration for image representation invariant to shading, shadows, lighting, and specularities," in *Proceedings of the Eighth IEEE International Conference on Computer Vision (IEEE 2001)*, pp. 473–480.
7. S. Ratnasingam and S. Collins "Study of the photodetector characteristics of a camera for color constancy in natural scenes," *J. Opt. Soc. Am. A* **27**, 286–294, 2010.
8. http://www.ccrs.nrcan.gc.ca/resource/tutor/fundam/chapter4/01_e.php.
9. S. Ratnasingam, S. Collins, and J. Hernández-Andrés, "Optimum sensors for color constancy in scenes illuminated by daylight," *J. Opt. Soc. Am. A* **27**, 2198–2207 (2010).
10. S. Winkler and S. Susstrunk, "Visibility of noise in natural images," *Proc. SPIE* **5292**, 121–129 (2004).
11. "Database—Munsell colors matt," http://cs.joensuu.fi/~spectral/databases/download/munsell_spec_matt.htm.
12. S. E. J. Arnold, V. Savolainen, and L. Chittka, "FRoD: the floral reflectance spectra database," *Nat. Prec.*, <http://dx.doi.org/10.1038/npre.2008.1846.1> (2008).
13. J. Hernández-Andrés, J. Romero, J. L. Nieves, and R. L. Lee, Jr., "Color and spectral analysis of daylight in southern Europe," *J. Opt. Soc. Am. A* **18**, 1325–1335 (2001).

14. J. Romero, A. García-Beltrán, and J. Hernández-Andrés, "Linear bases for representation of natural and artificial illuminants," *J. Opt. Soc. Am. A* **14**, 1007–1014 (1997).
15. F. H. Imai, M. R. Rosen, and R. S. Berns, "Comparative study of metrics for spectral match quality," in *Proceedings of CGIV 2002: The First European Conference on Colour in Graphics Image and Vision* (Society for Imaging Science and Technology, 2002), pp. 492–496.
16. H. Laamanen, T. Jetsu, T. Jaaskelainen, and J. Parkkinen, "Weighted compression of spectral color information," *J. Opt. Soc. Am. A* **25**, 1383–1388 (2008).
17. M. A. López-Álvarez, J. Hernández-Andrés, Eva. M. Valero, and J. Romero, "Selecting algorithms, sensors and linear bases for optimum spectral recovery of skylight," *J. Opt. Soc. Am. A* **24**, 942–956 (2007).